Spatiotemporal Organization of Chemical Oscillators via Phase Separation

Jonathan Bauermann,[1,*] Giacomo Bartolucci,[2,3] and Artemy Kolchinsky[4,5,6]
[1]Department of Physics, Harvard University, Cambridge, Massachusetts 02138, USA
[2]Department of Condensed Matter Physics, Universitat de Barcelona, 08007 Barcelona, Spain
[3]Universitat de Barcelona Institute of Complex Systems (UBICS), Universitat de Barcelona, 08028 Barcelona, Spain
[4]ICREA-Complex Systems Lab, Universitat Pompeu Fabra, 08003 Barcelona, Spain
[5]Barcelona Collaboratorium for Modelling and Predictive Biology, Wellington 30, 08005 Barcelona, Spain
[6]Universal Biology Institute, University of Tokyo, 7-3-1 Hongo, Bunkyo-ku, Tokyo 113-0033, Japan

(Received 23 July 2025; accepted 12 March 2026; published 28 April 2026)

We develop a method for studying chemical oscillators in the presence of phase separation. Specifically, we define a dynamics at phase equilibrium by imposing timescale separation between slow reactions and fast diffusion. We show that colocalization of components can alter oscillator frequency and amplitude, and that it determines the stability of oscillations and fixed points. Although our method applies to general reaction networks with phase separation, we illustrate it on a concrete example of a three-component oscillator ("rock-paper-scissors" model) with two-phase coexistence. The analysis is validated with a spatial model, where relaxing the timescale separation between reactions and diffusion leads to waves of phase equilibria at mesoscopic scales.

DOI: 10.1103/shz6-7fj9

Introduction—The discovery of biomolecular condensates in the cytoplasm [1], believed to form via phase separation, has led to increasing interest in the role of phase separation in cell biology [2–5]. Biomolecular condensates have been associated with a variety of cellular functions, including compartmentalization of chemical reactions in space [6–8]. Phase separation, together with reactions, may have also played an important role in abiogenesis. In fact, more than a century ago, Oparin and Haldane speculated that chemically active droplets might have been the first "metabolic units" at the origin of life [9,10]. Nowadays, phase separation is also drawing attention in ecology as a potential mechanism for the formation of patchy ecosystems [11,12].

In the context of nonequilibrium chemical reactions, phase separation can influence reaction kinetics by partitioning space and affecting local concentrations of components. Conversely, reactions can control the emergence of phases by altering chemical concentrations. As a result, highly nontrivial phenomena can result from coupling phase separation to nonequilibrium reactions, including pattern formation [13,14], alteration of droplet composition [15–17], ripening [18–22], nucleation [23,24], division [25,26], and propulsion [27–29].

*Contact author: jbauermann@fas.harvard.edu

Phase separation may also play an important role in various oscillatory biomolecular processes. Indeed, oscillating droplets have been proposed as a mechanism for regulating rhythmic translation, orchestrating circadian clocks [30,31], and improving DNA repair efficiency and robustness [32]. Moreover, it has been shown that phase separation can trigger oscillations [33,34], and that strong phase separation between all components of a cyclic reaction network typically generates fascinating spatial patterns, such as oscillating lattices of different phases with reactions occurring predominantly at phase boundaries [35]. However, a general framework to decipher the interplay between phase separation and the temporal organization of oscillatory reaction networks [36] is still lacking. To address this gap, we study how a nonequilibrium oscillator is modified by colocalization of components in coexisting phases. Specifically, we analyze the effects of phase separation in a simple but illustrative nonlinear oscillator, where the colocalization of chemical components via phase separation allows for targeted control of oscillator frequency and amplitude. Our techniques can be used to study any reaction network and to investigate multiphase coexistence. In general, this Letter shows how phase separation controls the stability of cycles and fixed points in nonlinear reaction networks.

Chemical oscillator—Oscillatory behavior is a hallmark of nonequilibrium dynamics, emerging in systems from chemical reactions to ecological predator-prey cycles. In this Letter, we use the simplest nonlinear reaction network, the rock-paper-scissors (RPS) model, which exhibits oscillations due to cyclic dominance [37–39]. It consists of three

components, A, B, C, that undergo a cycle of irreversible reactions,

$$A + B \xrightarrow{k_{AB}} 2A, \qquad B + C \xrightarrow{k_{BC}} 2B, \qquad C + A \xrightarrow{k_{CA}} 2C, \quad (1)$$

with second-order rate constants k_{ij}. This is a paradigmatic model in nonequilibrium statistical physics, exhibiting self-sustained oscillations, coexistence, and spatiotemporal pattern formation [40–42]. It has also been used to model dynamics of living systems, such as side-blotched lizards and *E. coli* populations [43–45], some of which are known to exhibit phenomena similar to phase separation [46–48]. Importantly, this oscillator has been realized in a chemical system based on interacting DNA strands [49].

The well-mixed ideal system is characterized by average (volume) concentrations $\boldsymbol{\rho} = (\rho_A, \rho_B, \rho_C)$. Their deterministic dynamics, assuming standard mass-action kinetics, is

$$\frac{d\boldsymbol{\rho}}{dt} = \mathcal{R}(\boldsymbol{\rho}), \quad \mathcal{R}(\boldsymbol{\rho}) = \begin{bmatrix} k_{AB}\rho_A\rho_B - k_{CA}\rho_C\rho_A \\ k_{BC}\rho_B\rho_C - k_{AB}\rho_A\rho_B \\ k_{CA}\rho_C\rho_A - k_{BC}\rho_B\rho_C \end{bmatrix}. \quad (2)$$

The simplicity of the RPS model relies on the fact that, in addition to the conserved quantity given by the total concentration $\psi = \rho_A + \rho_B + \rho_C$, it also has the constant of motion $\rho_A^{k_{BC}}\rho_B^{k_{CA}}\rho_C^{k_{AB}}$, both of which are determined by the initial conditions. Thus, the dynamics is effectively one-dimensional, and every initial condition with strictly positive concentrations leads to a closed neutrally stable cycle, except for the fixed point at $\boldsymbol{\rho} = (k_{BC}, k_{CA}, k_{AB})\psi/(k_{AB} + k_{BC} + k_{CA})$. Therefore, the RPS system resembles a harmonic oscillator in that its state can always be described by a single phase variable. We stress that the RPS network was chosen here for its simplicity; nevertheless, the general findings and tools discussed in this Letter apply to more complicated oscillatory reaction networks. In the following, we set the rate constants as $k_{AB} = k_{BC} = k_{CA} = 1$.

Phase separation—To capture interactions between components, we use the Flory-Huggins free energy density, written in dimensionless units as

$$f(\boldsymbol{\rho}) = \sum_{i=S,A,B,C} \rho_i \ln \rho_i + \sum_{j=S,B,C} \chi_{Aj}\rho_A\rho_j, \quad (3)$$

where S is the solvent with concentration $\rho_S = 1 - \psi$. The first sum describes the entropic contribution of mixing, while the second sum describes energetic interactions between components that can lead to phase separation. In this Letter, we focus on cases where one component can phase separate, here chosen as A, while the others only colocalize in phases. Thus, we only consider interactions between A and components $j = S, B, C$, parametrized by interaction energies χ_{Aj}.

While the log-nonlinearities of the Flory-Huggins free energy do not allow for closed form expressions, they guarantee equilibria with finite positive concentrations. Simpler free energy models, like the Ginzburg-Landau free energy, can lead to nonphysical results but prove useful to derive analytical expressions (e.g., linear stability analysis) as shown in Supplemental Material (SM) [50].

Reaction dynamics in phase-separating systems are usually studied in spatial models with local equilibrium [8], where each location $\boldsymbol{x}$ in volume V is associated with a local concentration vector $\boldsymbol{\rho}(\boldsymbol{x})$. The total free energy of a system, $F = \int_V d\boldsymbol{x}[f + (\nabla\boldsymbol{\rho})^T\boldsymbol{\kappa}\nabla\boldsymbol{\rho}/2]$, is an integral over the free energy density f and the contributions of spatial concentration gradients, parametrized by κ_{ij}. These parameters encode the effect of surface tension; for details see Refs. [51–53]. Spatial gradients of the local chemical potentials $\mu_i(\boldsymbol{x}) = \delta F/\delta\rho_i(\boldsymbol{x})$ drive diffusive fluxes. The deterministic dynamics of components $i = A, B, C$ then read [54,55]

$$\partial_t\boldsymbol{\rho}(\boldsymbol{x}) = \nabla \cdot [\boldsymbol{\Gamma}(\boldsymbol{x})\nabla\boldsymbol{\mu}(\boldsymbol{x})] + \mathcal{R}[\boldsymbol{\rho}(\boldsymbol{x})]. \quad (4)$$

We choose $\Gamma_{ij} = \gamma\rho_i(\delta_{ij} - \rho_j)$ as the mobility matrix with mobility coefficient γ, such that the diffusion term in Eq. (4) reduces to Fick's law when interactions χ_{Ai} and gradient terms κ_{ij} vanish [56,57]. In this case Eq. (4) reduces to the classical reaction-diffusion equation for the RPS dynamics [40,58,59]. For details of the parameter values, see SM [50].

In the absence of interactions, diffusion always reduces spatial inhomogeneities and dampens oscillations in deterministic systems. We show this using a global stability analysis of the RPS systems (with general diagonal diffusivity matrices) in SM [50]. In contrast, for the spatial dynamics in Eq. (4), which accounts for interactions, oscillations can grow once the interactions in Eq. (3) are sufficiently strong, such that concentration fields exhibit phase separation. As detailed in SM [50], we choose χ_{AS} to be sufficiently large so that two phases form: an A-rich phase I and an A-poor phase II. We set χ_{AB} and χ_{AC} sufficiently small so that B and C only localize inside or outside the two phases, but do not give rise to additional phases. Depending on whether $\chi_{AB} < 0$, $\chi_{AB} = 0$, or $\chi_{AB} > 0$, the concentration of B is higher, equal, or lower (respectively) in phase I, and similarly for χ_{AC} and C.

In Fig. 1(a), we show the spatial concentration profiles of A, B, and C from a typical trajectory of the spatial model in two dimensions, assuming fast diffusion and slow reactions. We show five time points within one period of an oscillation (left), illustrating nucleation, growth, shrinking, and dissolution of droplets. Moreover, we sketch the spatially averaged concentrations at these time points in the concentration space (right), showing how the system cycles through the region of high A concentrations where droplets can form (shaded in gray).

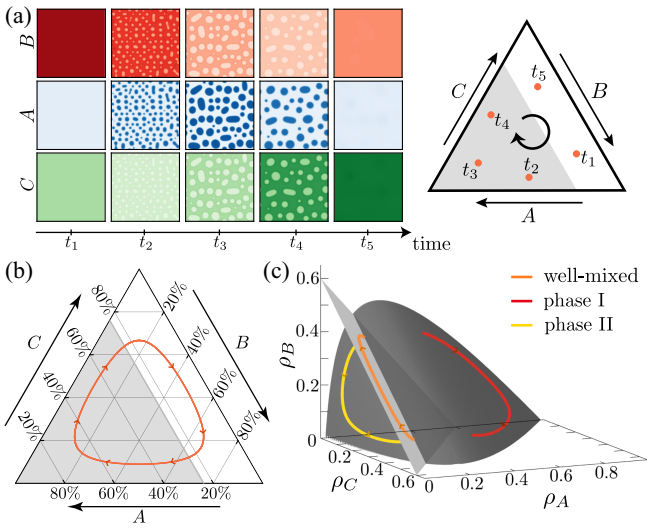

FIG. 1. Chemical oscillator in the presence of coexisting phases. (a) Spatial profiles (left) of $\boldsymbol{\rho}$ and corresponding spatial averages sketched in concentration space (right) at five time points in a spatial model. (b) Trajectory of average (volume) concentrations $\boldsymbol{\rho}$ in concentration space (orange). Within the binodal domain (gray shaded), phases coexist at equilibrium; outside the binodal domain (white), equilibrium is well-mixed. (c) Trajectories of $\boldsymbol{\rho}$ (orange) outside the binodal, and phase concentrations $\boldsymbol{\rho}^{\mathrm{I}}$ (red) and $\boldsymbol{\rho}^{\mathrm{II}}$ (yellow) at the binodal. Dark gray: binodal manifold; light gray: plane of constant total concentration ψ. Parameters: (a) $\chi_{AS} = 4, \chi_{AB} = \chi_{AC} = 1$; see Fig. 6 for further details. (b),(c) $\psi = 0.6$, $\chi_{AS} = 4$, $\chi_{AB} = \chi_{AC} = 0$.

In spatial models with phase separation, reaction dynamics can be solved using numerical techniques. However, this approach is computationally intensive and introduces complexities, such as interface effects and nucleation barriers. In particular, as explained below, homogeneous solutions are metastable for some concentrations, and fluctuations in Eq. (4) are required to nucleate droplets. Finally, the spatial model is difficult to analyze, for instance, to study stability analysis at phase equilibrium.

To circumvent these difficulties, in the following we consider reaction dynamics at global phase equilibrium. This leads to a low-dimensional system that is numerically and analytically tractable, allowing us to gain insight into the control of chemical oscillations through phase separation. We compare results from the coarse-grained model and the spatial models in End Matter and, at the end of this Letter, we examine cases where diffusion and reactions occur on similar timescales.

Reaction dynamics at phase equilibrium—Ideal systems are well-mixed when diffusion is fast compared to reactions. Analogously, we consider nonideal systems, in which fast diffusion establishes a global phase equilibrium instantaneously on the reaction timescale. Given an average concentration $\boldsymbol{\rho}$, phase separation is favored whenever there exist two phases, with concentrations $\boldsymbol{\rho}^{\mathrm{I/II}}$ and relative volume $v \in [0, 1]$ of phase I, such that $\boldsymbol{\rho} = v\boldsymbol{\rho}^{\mathrm{I}} + (1 - v)\boldsymbol{\rho}^{\mathrm{II}}$ (conservation law) and $vf(\boldsymbol{\rho}^{\mathrm{I}}) + (1 - v)f(\boldsymbol{\rho}^{\mathrm{II}}) \leq f(\boldsymbol{\rho})$ (lower average free energy). The boundary of the domain of $\boldsymbol{\rho}$ in which phase separation is favored is called the "binodal." Within this region, the seven equilibrium values of $(v, \boldsymbol{\rho}^{\mathrm{I}}, \boldsymbol{\rho}^{\mathrm{II}})$ are obtained by minimizing the average free energy subject to the conservation law [60,61].

Within the binodal, reactions occur in each phase, so the average concentration $\boldsymbol{\rho}$ evolves as [62]

$$\frac{d\boldsymbol{\rho}}{dt} = v(\boldsymbol{\rho})\mathcal{R}(\boldsymbol{\rho}^{\mathrm{I}}(\boldsymbol{\rho})) + (1 - v(\boldsymbol{\rho}))\mathcal{R}(\boldsymbol{\rho}^{\mathrm{II}}(\boldsymbol{\rho})). \tag{5}$$

This dynamics is closed, because for any given $\boldsymbol{\rho}$ at a specific time, the concentrations $\boldsymbol{\rho}^{\mathrm{I/II}}$ (at which the reaction fluxes are evaluated) and the relative phase volume v are uniquely defined at phase equilibrium. Moreover, as shown in End Matter, the dynamics of $v, \boldsymbol{\rho}^{\mathrm{I}}, \boldsymbol{\rho}^{\mathrm{II}}$ at phase equilibrium can be found in closed form. The full dynamics evolves as follows: whenever the average concentration $\boldsymbol{\rho}$ is within the binodal domain, Eq. (5) is used; once $\boldsymbol{\rho}$ leaves the binodal domain, the dynamics of the average follow Eq. (2).

We illustrate this dynamics in Figs. 1(b) and 1(c) for the special case $\chi_{AB} = \chi_{AC} = 0$. For these parameters, B and C do not localize preferentially in either phase, and remain homogeneously distributed. Because the RPS fluxes are linear in the concentration of each individual component, the dynamics in Eq. (5) differ from Eq. (2) only when two or more components (not only A) have unequal concentrations between the phases. Therefore, when $\chi_{AB} = \chi_{AC} = 0$, the average concentrations $\boldsymbol{\rho}$ undergo the same trajectory for all values of χ_{AS}, shown in Fig. 1(b). This average concentration trajectory is identical to the trajectory of the well-mixed dynamics, Eq. (2).

Figure 1(c) shows the dynamics in the three-dimensional phase space of the concentrations $\boldsymbol{\rho}$. Outside of the binodal domain, the trajectory (orange line) lies within the plane of constant ψ (light gray). However, when the oscillation enters the binodal domain (dark gray), the trajectories of $\boldsymbol{\rho}^{\mathrm{I}}$ (red) and $\boldsymbol{\rho}^{\mathrm{II}}$ (yellow) separate and run along the binodal manifold. As mentioned above, the dynamics of the well-mixed RPS model is effectively one-dimensional. When phases coexist, no constant of motion exists, and the dynamics can explore the entire two-dimensional space permitted by the conserved quantity ψ.

Phase separation controls the oscillations—Phase separation can localize B and C in the A-rich and A-poor phases. In turn, this can accelerate or decelerate reactions in the corresponding phases, resulting in changes in oscillator amplitude and frequency. The fact that oscillator amplitude and frequency can be controlled via phase separation is a key finding of our Letter. In the following section, we study this phenomenon quantitatively and discuss the underlying physical mechanism.

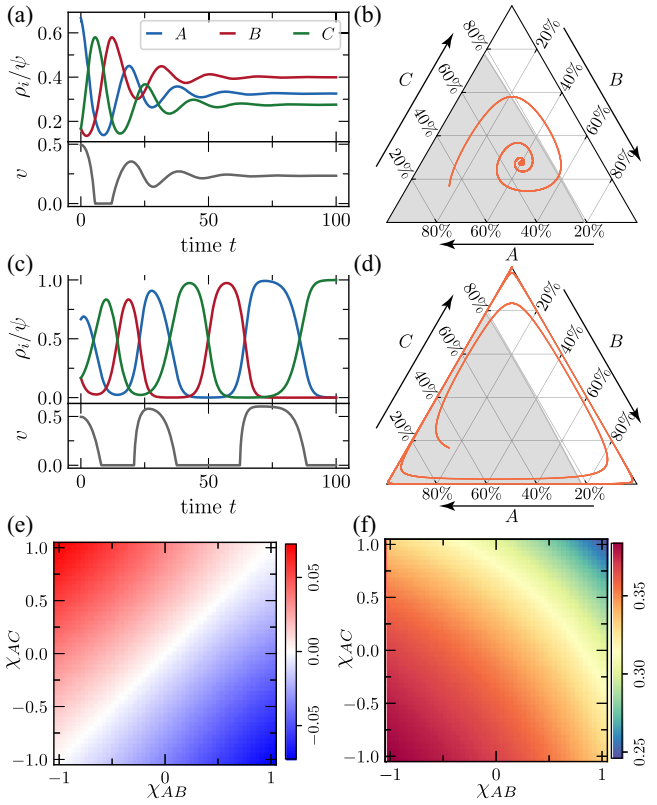

FIG. 2. Phase separation controls oscillations. (a),(c) Oscillations of the average concentrations $\boldsymbol{\rho}$ and volume v. (b),(d) Trajectories of the average concentrations, with the region within binodal in gray. (a),(b) For $\chi_{AB}=1,\chi_{AC}=-1$, oscillations are damped. (c),(d) For $\chi_{AB}=-1,\chi_{AC}=1$, oscillations are enhanced. (e),(f) Real and imaginary parts of the complex eigenvalues $\lambda_{\mathrm{Re}} \pm \mathbf{i}\lambda_{\mathrm{Im}}$ governing the linear stability of the fixed point of Eq. (5), as functions of χ_{AB} and χ_{AC}. (e) λ_{Re} captures the growth/decay rate; (f) λ_{Im} captures the oscillatory frequency. For all figures, $\psi=0.6$, $\chi_{AS}=4$.

We illustrate the interplay of phase separation and oscillations for different values of χ_{AB},χ_{AC} in Figs. 2(a)–2(d). When B localizes in the A-poor phase and C localizes in the A-rich phase ($\chi_{AB}>0,\chi_{AC}<0$), the oscillation is damped [Figs. 2(a) and 2(b)]. For the chosen initial conditions, the average concentration $\boldsymbol{\rho}$ (orange) only leaves the binodal domain [gray in Fig. 2(b)] in the first oscillation, leading to a transient where the volume of the A-rich phase v vanishes [bottom of Fig. 2(a)]. Afterward, the dynamics settles at a stationary state with coexisting phases ($0<v<1$). However, when B localizes in the A-rich phase and C in the A-poor one ($\chi_{AB}<0,\chi_{AC}>0$), the oscillation amplitude increases over time, and there are longer and longer intervals in which the mixture is composed mainly of a single solute, i.e., $\psi\sim\rho_i$; see Figs. 2(c) and 2(d). Such a trajectory, where the oscillator is pulled in turn toward each corner of the concentration space while its period keeps increasing, is known as a heteroclinic cycle [37].

To give insight on how interactions control oscillator properties, we compute the linear stability of the fixed point of the dynamics. We focus on parameter regimes for which the fixed point is located within the binodal domain, i.e., involves phase separation. The stability is determined by the two eigenvalues of the Jacobian at the fixed point, which have the form $\lambda_{\mathrm{Re}} \pm \mathbf{i}\lambda_{\mathrm{Im}}$ (see End Matter). In general, finding the fixed point of Eq. (5) and its corresponding phase equilibrium must be done numerically. Once the fixed point concentrations are found, the eigenvalues can be computed in closed form.

In Figs. 2(e) and 2(f), we show the real and imaginary parts of these eigenvalues λ_{Re} and λ_{Im} in the space of χ_{AB} and χ_{AC}. The sign of (λ_{Re}) predicts that perturbations grow when ($\chi_{AB}<\chi_{AC}$), are marginally stable when ($\chi_{AB}=\chi_{AC}$), and are damped when ($\chi_{AB}>\chi_{AC}$). The magnitude of the imaginary part controls the frequency of the oscillations. The lower the values χ_{AB} and χ_{AC}, the faster the system oscillates. These findings are consistent with the examples shown in Fig. 2.

The influence of localization on the frequency and amplitude can be explained as follows: due to our choice of interactions, A drives phase separation such that $|\rho_A^{\mathrm{I}}-\rho_A^{\mathrm{II}}|\gg|\rho_j^{\mathrm{I}}-\rho_j^{\mathrm{II}}|$ for $j=B,C$. For this reason, the presence of phases mainly affects the reactions that involve A ($A+B\to 2A$ and $C+A\to 2C$) and has less influence on the third reaction ($B+C\to 2B$). If B localizes in the A-rich phase ($\chi_{AB}<0$), the reaction $A+B\to 2A$ is accelerated and produces on average more A than in the well-mixed system [compare Eq. (2) with Eq. (5)]; conversely, when $\chi_{AB}>0$, the reaction is decelerated and production of A decreases. Localization of C in the A-rich phase ($\chi_{AC}<0$) accelerates and enhances the decay of A via the reaction $C+A\to 2C$; conversely, when $\chi_{AC}>0$, the reaction is slowed and decay of A decreases. For this reason, when $\chi_{AB}<0,\chi_{AC}<0$, the production and the decay of A are accelerated, leading to a faster oscillation; as they become positive, the frequency decreases. In addition, when $\chi_{AB}<\chi_{AC}$, there is a net increase in A in each cycle, leading to amplification of oscillations; when $\chi_{AB}>\chi_{AC}$, A decreases in every cycle, damping the oscillations.

For any reaction network, eigenvalue scaling relations can be deduced from the symmetries of the free energy function and the reaction kinetics. In the SM [50], we consider how the eigenvalues change when the interaction energies χ_{AB} and χ_{AC} are swapped. We show that λ_{Im} is unchanged (the oscillatory frequency around the fixed point remains the same), while λ_{Re} changes sign (the stability of the fixed point flips). These symmetries imply simple scaling relations of the eigenvalue in the total strength $\Sigma=\chi_{AB}+\chi_{AC}$ and asymmetry $\xi=\chi_{AB}-\chi_{AC}$ of interactions. Specifically, under weak smoothness assumptions, we may expand

$$\lambda_{\mathrm{Re}}=c_{\mathrm{r}}^{10}\xi+c_{\mathrm{r}}^{11}\Sigma\xi,\qquad \lambda_{\mathrm{Im}}=c_{\mathrm{i}}^{00}+c_{\mathrm{i}}^{01}\Sigma+c_{\mathrm{i}}^{20}\xi^2+c_{\mathrm{i}}^{02}\Sigma^2,$$

up to second order with the Taylor coefficients c_{r}^{nm} and c_{i}^{nm}. Furthermore, $c_{\mathrm{i}}^{00} = \psi/\sqrt{3}$ is the same frequency as for the well-mixed system in the absence of phase separation. These predictions are confirmed numerically in Fig. 2(e), which is antisymmetric about the diagonal, and Fig. 2(f), which is symmetric. We derive these coefficients for a simpler model of a Ginzburg-Landau free energy density in SM [50]. So far, we studied fixed points within the binodal domain, showing that colocalization can change their stability. However, if the fixed point lies outside of the binodal, phase separation can control the amplitude of oscillations (see End Matter).

Before returning to spatial systems, let us briefly address fluctuations. Our analysis above assumed instantaneous phase equilibration upon entering the binodal domain, i.e., droplet nucleation is much faster than reactions. To model metastability due to slow nucleation, one may impose the onset of phase separation only at the boundary of the spinodal region, where a finite nucleation size is not necessary for phase separation. In systems with fluctuations, phase formation typically occurs between the binodal and spinodal lines (see End Matter).

Fast reactions—In our final analysis, we demonstrate how phases change spatial dynamics in systems where reaction and diffusion have comparable timescales. As mentioned above, in the absence of interactions, diffusion dampens oscillations in deterministic RPS systems (chemical waves can persist for more complicated reaction schemes, stochastic dynamics, or cross-diffusion of the components [40,50,58,59,63,64]).

Here, we demonstrate numerically that the localization of components within droplets can give rise to persistent chemical waves on length scales exceeding the droplet sizes. Furthermore, the stability analysis of the reaction network at phase coexistence can predict for which interaction energies these waves occur; see Sec. II E in SM [50].

We consider the spatial model (4), initialized with random concentration fields so that locally the oscillations are at different phases [50]. Whenever the average concentration of ρ_A is high in a mesoscopic region, droplets form in this domain.

For interaction parameters $\chi_{AB} > \chi_{AC}$, the colocalization of B and C into these droplets dampens the oscillations. Thus, on this mesoscopic scale, a stationary state is reached where diffusive fluxes between phases counterbalance the reaction fluxes between components, corresponding to the attracting fixed point of Eq. (5). Eventually, the same stationary state is reached everywhere in the system, corresponding to an effective global phase equilibrium.

However, for interaction parameters $\chi_{AB} < \chi_{AC}$, the colocalization of B and C into droplets amplifies oscillations. At the frontier of A-rich waves, droplets nucleate locally, grow, and further amplify the reactions until they dissolve as the wave travels further. This is illustrated in Fig. 3(a), where we show concentration fields at one time (see also the movie [50]).

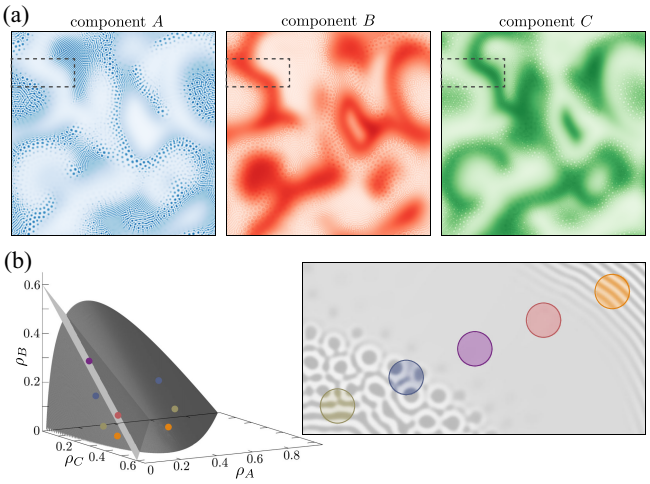

FIG. 3. Mesoscopic waves of phase equilibria emerge in the fast reaction regime. (a) Spatial concentrations in a large system. (b) Right: local total concentration ψ in an enlarged region of space (gray dashed box in top plots). Average concentrations in five mesoscopic environments (colored circles on the right) are shown in concentration space (left), together with the binodal (dark gray) and the plane of conserved ψ (light gray). $\psi = 0.6$, $\chi_{AS} = 4$, $\chi_{AB} = -1$, $\chi_{AC} = 1$; see the End Matter for details.

In Fig. 3(b), we illustrate how different phase equilibria are selected within these waves. On the right, we show the field of the conserved quantity ψ for an enlarged region of the system [dashed box in Fig. 3(a)]. Within this region, we determine the average concentrations in mesoscopic environments (colored spots) that are smaller than the length scale of the traveling waves. Using a standard clustering algorithm [65], we identify whether there are two distinct phases and their corresponding average concentrations. On the left, we display these phase concentrations in their corresponding colors, together with the equilibrium phase diagram. In these local environments, the concentrations lie on the binodal manifold whenever the wave is in an A-rich domain. However, in the domains that are rich in B and C, the system is well-mixed and the concentration lies on the plane of constant ψ (light gray).

Conclusion—We demonstrate that phase separation modifies oscillator dynamics by changing amplitude and frequency of oscillations, and even controlling the stability of cycles and fixed points. To derive our results, we introduce stability analysis at phase equilibrium, which may be considered the analog of the mean-field stability analysis in classical reaction-diffusion systems. In addition, we show that phase separation can control the spatiotemporal organization of spatial systems, where different phase equilibria can coexist simultaneously at different parts of traveling waves. Our analysis of spatial systems contributes to recent work on identifying local equilibria in active matter [66–69].

For concreteness and simplicity, we focus on the canonical case of RPS dynamics. Experimental validation of our quantitative predictions may be achieved by combining existing experimental setups, such as DNA-based implementations of RPS dynamics [49] and controllable phase separation [70]. However, our qualitative results regarding the interplay between phase separation and oscillations have implications for a much broader range of systems, including in biology where oscillations in combination with phase separation have been observed *in vivo* in circadian clocks [30,31].

Acknowledgments—A. K. and G. B. thank the Barcelona Collaboratorium for encouraging fruitful discussions. J. B. thanks the German Research Foundation for financial support through the DFG Project BA 8210/1-1. G. B. thanks the Agencia Estatal de Investigación for funding through the Juan de la Cierva postdoctoral programme JDC2023-051554-I. A. K. is partly supported by John Templeton Foundation (Grant No. 62828) and by the European Union's Horizon 2020 research and innovation programme under the Marie Skłodowska-Curie Grant Agreement No. 101068029.

Data availability—The data that support the findings of this article are openly available [71].

[1] C. P. Brangwynne, C. R. Eckmann, D. S. Courson, A. Rybarska, C. Hoege, J. Gharakhani, F. Jülicher, and A. A. Hyman, Science **324**, 1729 (2009).
[2] S. F. Banani, H. O. Lee, A. A. Hyman, and M. K. Rosen, Nat. Rev. Mol. Cell Biol. **18**, 285 (2017).
[3] S. Boeynaems, S. Alberti, N. L. Fawzi, T. Mittag, M. Polymenidou, F. Rousseau, J. Schymkowitz, J. Shorter, B. Wolozin, L. Van Den Bosch, P. Tompa, and M. Fuxreiter, Trends Cell Biol. **28**, 420 (2018).
[4] A. A. Hyman, C. A. Weber, and F. Jülicher, Annu. Rev. Cell Dev. Biol. **30**, 39 (2014).
[5] D. M. Mitrea and R. W. Kriwacki, Cell Commun. Signaling **14**, 1 (2016).
[6] C. A. Strulson, R. C. Molden, C. D. Keating, and P. C. Bevilacqua, Nat. Chem. **4**, 941 (2012).
[7] K. K. Nakashima, M. A. Vibhute, and E. Spruijt, Front. Mol. Biosci. **6**, 21 (2019).
[8] C. A. Weber, D. Zwicker, F. Jülicher, and C. F. Lee, Rep. Prog. Phys. **82**, 064601 (2019).
[9] A. Oparin, *The Origin of Life* (Dover Publications, New York, 1953).
[10] J. B. S. Haldane, Rationalist Annu. **148**, 3 (1929).
[11] Q.-X. Liu, A. Doelman, V. Rottschäfer, M. de Jager, P. M. Herman, M. Rietkerk, and J. van de Koppel, Proc. Natl. Acad. Sci. U.S.A. **110**, 11905 (2013).
[12] K. Siteur, Q.-X. Liu, V. Rottschäfer, T. van der Heide, M. Rietkerk, A. Doelman, C. Boström, and J. van de Koppel, Proc. Natl. Acad. Sci. U.S.A. **120**, e2202683120 (2023).
[13] T. Aslyamov, F. Avanzini, É. Fodor, and M. Esposito, Phys. Rev. Lett. **131**, 138301 (2023).
[14] F. Avanzini, T. Aslyamov, É. Fodor, and M. Esposito, J. Chem. Phys. **161**, 174108 (2024).
[15] J. Kirschbaum and D. Zwicker, J. R. Soc. Interface **18**, 20210255 (2021).
[16] Y. Cho and W. M. Jacobs, J. Chem. Phys. **159**, 154101 (2023).
[17] S. Laha, J. Bauermann, F. Jülicher, T. C. T. Michaels, and C. A. Weber, Phys. Rev. Res. **6**, 043092 (2024).
[18] S. C. Glotzer, E. A. Di Marzio, and M. Muthukumar, Phys. Rev. Lett. **74**, 2034 (1995).
[19] D. Zwicker, A. A. Hyman, and F. Jülicher, Phys. Rev. E **92**, 012317 (2015).
[20] J. D. Wurtz and C. F. Lee, Phys. Rev. Lett. **120**, 078102 (2018).
[21] A. Kumar and S. A. Safran, Phys. Rev. Lett. **131**, 258401 (2023).
[22] J. Bauermann, G. Bartolucci, C. A. Weber, and F. Jülicher, Phys. Rev. Lett. **135**, 148201 (2025).
[23] N. Ziethen, J. Kirschbaum, and D. Zwicker, Phys. Rev. Lett. **130**, 248201 (2023).
[24] Y. Cho and W. M. Jacobs, Phys. Rev. Lett. **130**, 128203 (2023).
[25] D. Zwicker, R. Seyboldt, C. A. Weber, A. A. Hyman, and F. Jülicher, Nat. Phys. **13**, 408 (2017).
[26] J. Bauermann, C. A. Weber, and F. Jülicher, Ann. Phys. (Amsterdam) **534**, 2200132 (2022).
[27] L. Demarchi, A. Goychuk, I. Maryshev, and E. Frey, Phys. Rev. Lett. **130**, 128401 (2023).
[28] G. Häfner and M. Müller, ACS Nano **18**, 16530 (2024).
[29] A. Goychuk, arXiv:2506.07753.
[30] Y. Zhuang, Z. Li, S. Xiong, C. Sun, B. Li, S. A. Wu, J. Lyu, X. Shi, L. Yang, Y. Chen *et al.*, Cell **186**, 3245 (2023).
[31] D. Tariq, N. Maurici, B. M. Bartholomai, S. Chandrasekaran, J. C. Dunlap, A. Bah, and B. R. Crane, eLife **12**, RP90259 (2024).
[32] M. S. Heltberg, A. Lucchetti, F.-S. Hsieh, D. P. M. Nguyen, S.-h. Chen, and M. H. Jensen, Cell **185**, 4394 (2022).
[33] I. S. Haugerud, H. D. Vuijk, J. Boekhoven, and C. A. Weber, arXiv:2503.11604.
[34] J. Sastre, A. Thatte, A. M. Bergmann, M. Stasi, M. Tena-Solsona, C. A. Weber, and J. Boekhoven, Nat. Commun. **16**, 2003 (2025).
[35] C. Luo and D. Zwicker, Phys. Rev. E **108**, 034206 (2023).
[36] I. B. A. Smokers, B. S. Visser, W. P. Lipiński, K. K. Nakashima, and E. Spruijt, ChemSystemsChem **7**, e202400056 (2024).
[37] R. M. May and W. J. Leonard, SIAM J. Appl. Math. **29**, 243 (1975).
[38] J. Hofbauer and K. Sigmund, *Evolutionary Games and Population Dynamics* (Cambridge University Press, Cambridge, England, 1998).
[39] J. M. Smith, *Evolution and the Theory of Games* (Cambridge University Press, Cambridge, England, 2012).
[40] T. Reichenbach, M. Mobilia, and E. Frey, Nature (London) **448**, 1046 (2007).
[41] M. Mobilia, J. Theor. Biol. **264**, 11 (2010).
[42] G. Szabó and G. Fáth, Phys. Rep. **446**, 97 (2007).
[43] B. Sinervo and C. M. Lively, Nature (London) **380**, 240 (1996).
[44] B. Kerr, M. A. Riley, M. W. Feldman, and B. J. M. Bohannan, Nature (London) **418**, 171 (2002).

[45] M. J. Liao, M. O. Din, L. Tsimring, and J. Hasty, Science **365**, 1045 (2019).
[46] S. C. Takatori and J. F. Brady, Phys. Rev. E **91**, 032117 (2015).
[47] M. E. Cates and J. Tailleur, Annu. Rev. Condens. Matter Phys. **6**, 219 (2015).
[48] A. P. Solon, J. Stenhammar, M. E. Cates, Y. Kafri, and J. Tailleur, Phys. Rev. E **97**, 020602(R) (2018).
[49] N. Srinivas, J. Parkin, G. Seelig, E. Winfree, and D. Soloveichik, Science **358**, eaal2052 (2017).
[50] See Supplemental Material at http://link.aps.org/supplemental/10.1103/shz6-7fj9 for details.
[51] J. W. Cahn and J. E. Hilliard, J. Chem. Phys. **28**, 258 (1958).
[52] G. I. Tóth, T. Pusztai, and L. Gránásy, Phys. Rev. B **92**, 184105 (2015).
[53] G. I. Tóth, M. Zarifi, and B. Kvamme, Phys. Rev. E **93**, 013126 (2016).
[54] L. Onsager, Phys. Rev. **37**, 405 (1931).
[55] S. R. De Groot and P. Mazur, *Non-Equilibrium Thermodynamics*, Dover Books on Physics (Dover Publications, Mineola, NY, 2003).
[56] E. J. Kramer, P. Green, and C. J. Palmstrøm, Polymer **25**, 473 (1984).
[57] S. Bo, L. Hubatsch, J. Bauermann, C. A. Weber, and F. Jülicher, Phys. Rev. Res. **3**, 043150 (2021).
[58] T. Reichenbach, M. Mobilia, and E. Frey, J. Theor. Biol., **254** 368 (2008).
[59] Q. He, M. Mobilia, and U. C. Täuber, Phys. Rev. E **82**, 051909 (2010).
[60] S. Safran, *Statistical Thermodynamics of Surfaces, Interfaces, and Membranes* (CRC Press, London, 2019).
[61] M. Kardar, *Statistical Physics of Fields* (Cambridge University Press, Cambridge, England, 2007).
[62] J. Bauermann, S. Laha, P. M. McCall, F. Jülicher, and C. A. Weber, J. Am. Chem. Soc. **144**, 19294 (2022).
[63] M. Peltomäki and M. Alava, Phys. Rev. E **78**, 031906 (2008).
[64] B. Szczesny, M. Mobilia, and A. M. Rucklidge, Phys. Rev. E **90**, 032704 (2014).
[65] F. Pedregosa, G. Varoquaux, A. Gramfort, V. Michel, B. Thirion, O. Grisel, M. Blondel, P. Prettenhofer, R. Weiss, V. Dubourg, J. Vanderplas, A. Passos, D. Cournapeau, M. Brucher, M. Perrot, and E. Duchesnay, J. Mach. Learn. Res. **12**, 2825 (2011).
[66] J. Halatek and E. Frey, Nat. Phys. **14**, 507 (2018).
[67] J. Halatek, F. Brauns, and E. Frey, Phil. Trans. R. Soc. B **373**, 20170107 (2018).
[68] A. W. Fritsch, A. F. Diaz-Delgadillo, O. Adame-Arana, C. Hoege, M. Mittasch, M. Kreysing, M. Leaver, A. A. Hyman, F. Jülicher, and C. A. Weber, Proc. Natl. Acad. Sci. U.S.A. **118**, e2102772118 (2021).
[69] J. F. Robinson, T. Machon, and T. Speck, Phys. Rev. E **111**, 065417 (2025).
[70] M. Tateno and O. A. Saleh, Phys. Rev. Lett. **136**, 068403 (2026).
[71] J. Bauermann, G. Bartolucci, and A. Kolchinsky, Data for reproducing the figures of the paper: "Spatiotemporal organization of chemical oscillators via phase separation" (2026), 10.5281/zenodo.18990195.
[72] S. H. Strogatz, *Nonlinear Dynamics and Chaos* (CRC Press, London, 2018).
[73] D. Deviri and S. A. Safran, Proc. Natl. Acad. Sci. U.S.A. **118**, e2100099118 (2021).
[74] C. Zechner and F. Jülicher, Cell Syst. **16**, 101168 (2025).
[75] A. Klosin, F. Oltsch, T. Harmon, A. Honigmann, F. Jülicher, A. A. Hyman, and C. Zechner, Science **367**, 464 (2020).
[76] A. Bray, Adv. Phys. **43**, 357 (1994).

End Matter

Closed-form dynamics at phase equilibrium—The dynamics at phase equilibrium can be written in closed form. Specifically, given the vector of phase equilibrium variables $\mathcal{E} = (v, \rho_A^{\mathrm{I}}, \rho_B^{\mathrm{I}}, \rho_C^{\mathrm{I}}, \rho_A^{\mathrm{II}}, \rho_B^{\mathrm{II}}, \rho_C^{\mathrm{II}})$, we write

$$d\mathcal{E}_i/dt = (\nabla_{\boldsymbol{\rho}}\mathcal{E}_i)\cdot(d\boldsymbol{\rho}/dt), \tag{A1}$$

where we use the partial derivatives $\nabla_{\boldsymbol{\rho}} = (\partial_{\rho_A}, \partial_{\rho_B}, \partial_{\rho_C})$. The latter can be computed using the following response formula:

$$\frac{\partial v}{\partial \rho_i} = \frac{\Delta^\top W \boldsymbol{e}_i}{\Delta^\top W \Delta}, \qquad \frac{\partial \boldsymbol{\rho}^{\mathrm{I/II}}}{\partial \rho_i} = H_{\mathrm{I/II}}^{-1} W \left[\boldsymbol{e}_i - \frac{\partial v}{\partial \rho_i}\Delta\right]. \tag{A2}$$

Here, we use the Hessians $H_{\mathrm{I}}/H_{\mathrm{II}}$ of the free energy density f at $\boldsymbol{\rho}^{\mathrm{I}}/\boldsymbol{\rho}^{\mathrm{II}}$, the matrix $W \coloneqq [vH_{\mathrm{I}}^{-1} + (1-v)H_{\mathrm{II}}^{-1}]^{-1}$, the concentration difference $\Delta \coloneqq \boldsymbol{\rho}^{\mathrm{I}} - \boldsymbol{\rho}^{\mathrm{II}}$, and the i th unit vector $\boldsymbol{e}_i$. For a derivation of Eq. (A2), see SM [50].

These expressions hold for any $\boldsymbol{\rho}$ within the binodal and any free energy density f. They allow us to efficiently track the dynamics as follows: when the average concentration $\boldsymbol{\rho}$ is within the binodal domain, the corresponding phase equilibrium $\mathcal{E}$ evolves according to Eq. (A1) (the initial phase equilibrium may be found by numerical optimization). Once $\boldsymbol{\rho}$ leaves the binodal domain, the dynamics of the average follow Eq. (2).

Linear stability analysis—The stability of the fixed point $\boldsymbol{\rho}^*$ is given by the two eigenvalues of the Jacobian matrix $\boldsymbol{M}$ [72]. To compute this matrix, we first note that $\psi = \rho_A + \rho_B + \rho_C$ is a conserved quantity, thus the fixed point with coexisting phases may be specified by 2 degrees of freedom. We perturb the fixed point $\boldsymbol{\rho}^*$ by the vector $(-\delta\rho_B - \delta\rho_C, \delta\rho_B, \delta\rho_C)$, which conserves ψ. To first order, the perturbation evolves as

$$\frac{d}{dt}\begin{bmatrix}\delta\rho_B\\ \delta\rho_C\end{bmatrix} = \boldsymbol{M}\begin{bmatrix}\delta\rho_B\\ \delta\rho_C\end{bmatrix}. \tag{B1}$$

Here, we introduced the 2×2 Jacobian

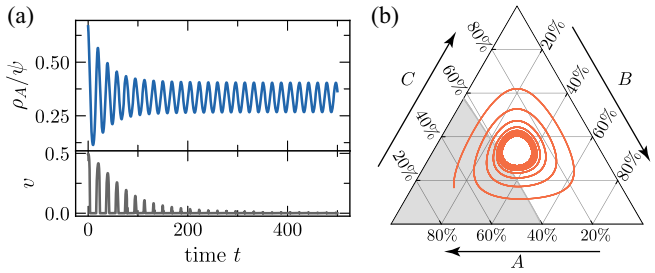

FIG. 4. Tuning of oscillation amplitude when the fixed point lies in the homogeneous domain: (a) Oscillations of the average concentrations ρ_A and relative volume v; (b) average concentration trajectory. $\psi = 0.6$, $\chi_{AS} = 3$, $\chi_{AB} = 1$, $\chi_{AC} = -1$.

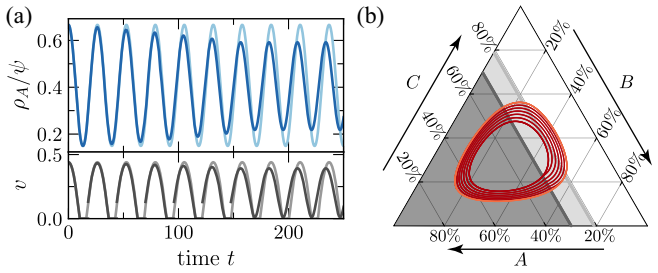

FIG. 5. Metastability affects oscillations. Without metastability, phases form when the binodal line is crossed (light colors); with metastability, phases form when the spinodal (darker colors) is crossed. (a) Oscillations of average concentration ρ_A and volume v. (b) Trajectory of average concentrations without (orange) and with (dark red) metastability. $\psi = 0.6$, $\chi_{AS} = 4$, $\chi_{AB} = 1$, $\chi_{AC} = 1$.

$$M_{ij} = \sum_{n=1,\ldots,7} \frac{\partial(d\rho_i/dt)}{\partial \mathcal{E}_n} \left(\frac{\partial \mathcal{E}_n}{\partial \rho_j} - \frac{\partial \mathcal{E}_n}{\partial \rho_A} \right) \Bigg|_{\boldsymbol{\rho}^*}, \qquad \text{(B2)}$$

with $i, j \in \{B, C\}$ and vector of phase-equilibrium variables $\mathcal{E}$. The derivatives $\partial \mathcal{E}_n / \partial \rho_j$ are given in Eq. (A2).

Fixed point outside the binodal domain—In the main text, we focused on situations where the fixed point of the dynamics lies within the binodal domain. However, for lower values of χ_{AS} or different values of ψ, the fixed point may lie outside of the binodal, where there is no phase separation. When the initial amplitude is large, such systems still undergo phase separation initially. When phase separation amplifies the oscillation amplitude ($\chi_{AC} > \chi_{AB}$), the system keeps on entering the binodal domain. However, for cases of damped oscillation ($\chi_{AB} > \chi_{AC}$), the amplitude decreases until the system oscillates without entering the binodal domain. We illustrate this in Fig. 4. For early times, the trajectory runs through the binodal domain, where the oscillation is damped, such that the relative volume v gets smaller in each period, as shown in Fig. 4(a). Eventually, the oscillation amplitude is sufficiently small such that the oscillation settles into a limit cycle outside the binodal line; see Fig. 4(b). This mechanism shows that phase separation can not only buffer concentrations at steady state [73,74], as demonstrated for biomolecular condensates in the cytosol [75], but can also buffer the amplitude of chemical oscillations.

Dynamics with metastability—For concentrations $\boldsymbol{\rho}$ in the outermost part of the binodal, also known as the "nucleation and growth" domain, spatially homogeneous states are metastable, and rare macroscopic fluctuations are required to form a droplet above a certain critical size. On the other hand, within the spinodal domain, the spatially homogeneous states are locally unstable and phase separation happens essentially instantaneously [76]. Formally, we may account for metastability by accompanying the two-dimensional dynamics with a third variable that tracks phase hysteresis induced by metastability. This variable enforces a switch from Eqs. (2) to (5) whenever the system is well-mixed and enters the spinodal domain, and a switch from Eqs. (5) to (2) whenever the system is phase-separated and leaves the binodal domain.

The presence of metastability affects oscillator dynamics, as shown in Fig. 5 for $\chi_{AB} = \chi_{AC} = 1$. Because of this choice of interactions, when phases are formed at the binodal (i.e., when metastability is not accounted for), oscillations have constant amplitude [ρ_A shown in light blue in Fig. 5(a)] and a closed trajectory [orange in Fig. 5(b)]. In contrast, metastability leads to a damped oscillation [ρ_A shown in dark blue in Fig. 5(a)], until the system reaches a limit cycle completely within the binodal domain such that there are always coexisting phases [dark orange in Fig. 5(b)]. Since $\chi_{AB} = \chi_{AC} > 0$, both production and decay of A are slowed down by the presence of phases. Because of the symmetry of the phase diagram and the reaction scheme, the effects cancel out, and the oscillation forms a closed cycle in the concentration space. However, this symmetry is broken when metastability of homogeneous phases is considered because the two processes predominate at different times within the oscillatory dynamics. The production of A occurs predominantly when the system enters the binodal domain, while the decay of A happens predominantly when the system leaves the binodal domain. When metastability of the homogeneous state is considered, the formation of phases, and therefore the deceleration of production of A, is delayed as long as the system is outside the spinodal domain [Fig. 5(b), dark gray]. However, once phases are formed, they are present as long as the system stays within the binodal domain [Fig. 5(b), light gray]. This asymmetry

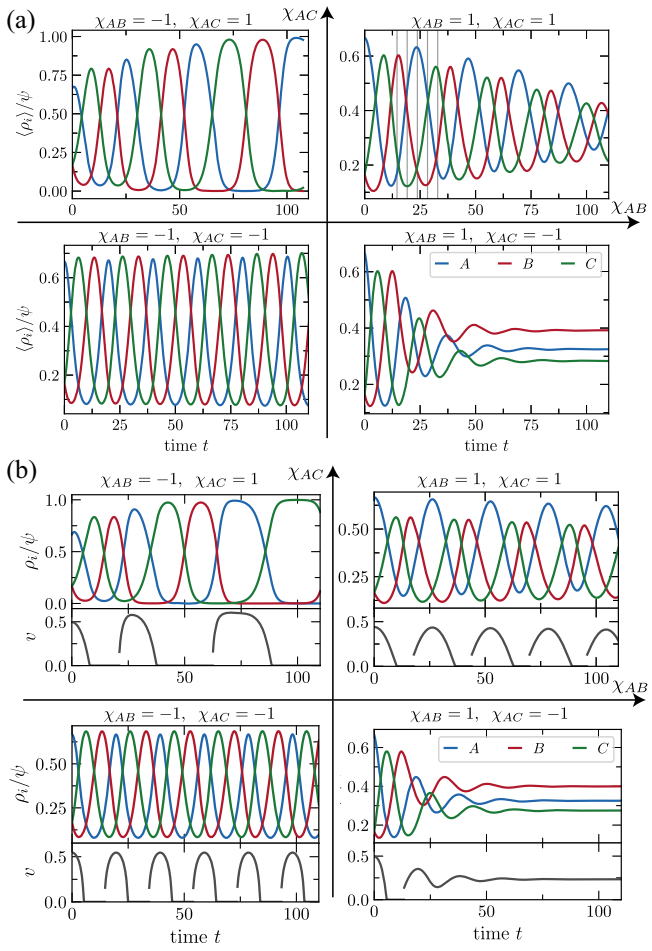

FIG. 6. Qualitative agreement between the dynamics at phase equilibrium and the spatial dynamics in the fast diffusion regime. Dynamics of the average concentrations $\boldsymbol{\rho}$ for four cases in a two-dimensional spatial model (a) and the dynamics at phase equilibrium (b). For the dynamics in (b), we have taken into account the metastability of homogeneous phases, leading to jumps in the relative phase volume v. The spatial concentration profiles at five time points [gray lines in (a), top right] are shown in Fig. 1; $\psi = 0.6$, $\chi_{AS} = 4$.

leads to an overall damping of the oscillation until the system remains fully within the binodal domain. Here, phases exist at all times of the oscillation, and the metastability of the homogeneous state is unimportant. On the other hand, for $\chi_{AB} = \chi_{AC} < 0$, metastability leads to amplification, rather than decay, of oscillations, giving rise to a heteroclinic cycle.

Comparison between spatial dynamics and dynamics at phase equilibrium—Here, we compare the dynamics at phase equilibrium with those in spatial models in the limit of fast diffusion. For this, we show the dynamics of the average concentrations $\langle \boldsymbol{\rho} \rangle = \int_V d\boldsymbol{x} \boldsymbol{\rho}(\boldsymbol{x}) / \int_V d\boldsymbol{x}$ of two-dimensional spatial fields and the coarse-grained ordinary differential equation model with metastability, as described in the main text and illustrated in Fig. 6. We consider four different systems, corresponding to each quadrant of the $\chi_{AB} - \chi_{AC}$ plane shown in Fig. 2.

Qualitatively, both dynamics exhibit the following behavior: for ($\chi_{AB} < 0, \chi_{AC} > 0$) (top left), the oscillation amplitude increases. In every oscillation, initially several droplets or stripes are nucleated and grow, but later they shrink and finally dissolve, such that the system becomes spatially homogeneous again. On the contrary, when $\chi_{AB} > 0, \chi_{AC} < 0$ (bottom right), after the first oscillation where all droplets dissolve, the system stays within the binodal regime and enters a stage where oscillations are suppressed and droplets slowly ripen. For the two cases $\chi_{AB} = \chi_{AC} > 0$ (top right) and $\chi_{AB} = \chi_{AC} < 0$ (bottom left), the amplitude of the oscillations slowly decreases or increases. This behavior is a result of the metastability. Nevertheless, the frequency of the oscillations for $\chi_{AB} = \chi_{AC} < 0$ is faster than for $\chi_{AB} = \chi_{AC} > 0$.

However, quantitatively, there are differences between the two dynamics. As mentioned in the main text, the full spatial model includes effects from interface regions, the Laplace pressure induced by curved interfaces, finite nucleation timescales even within the spinodal, and ripening of droplets.